Electro-optic Charon polymeric microring modulators

Daniele Rezzonico, Mojca Jazbinsek, Andrea Guarino, O-Pil Kwon, and Peter Günter

Nonlinear Optics Laboratory, Swiss Federal Institute of Technology, ETH Zurich, CH-8093 Zürich, Switzerland

nlo@nlo.ch

http://www.nlo.ch

Abstract: We propose and demonstrate a new type of electro-optic polymeric microring resonators, where the shape of the transmission spectrum is controlled by losses and phase shifts induced at the asymmetric directional coupler between the cavity and the bus waveguide. The theoretical analysis of such *Charon* microresonators shows, depending on the coupler design, three different transmission characteristics: normal Lorentzian dips, asymmetric Fano resonances, and Lorentzian peaks. The combination of the active azo-stilbene based polyimide SANDM2 surrounded by the hybrid polymer Ormocomp allowed the first experimental demonstration of electro-optic modulation in *Charon* microresonators. The low-loss modulators (down to 0.6 dB per round trip), with a radius of 50 μm, were produced by micro-embossing and exhibit either highly asymmetric and steep Fano resonances with large 43-GHz modulation bandwidth or strong resonances with 11-dB extinction ratio. We show that *Charon* microresonators can lead to 1-V half wave voltage all-polymer micrometer-scale devices with larger tolerances to coupler fabrication limitations and wider modulation bandwidths than classical ring resonators.

OCIS codes: (130.4110) Modulators; (230.2090) Electro-optical devices; (160.5470) Polymers

References and links

1. M. Lee, H.E. Katz, Ch. Erben, D.M. Gill, P. Gopalan, J.D. Heber, D.J. McGee, "Broadband modulation of light by using an electro-optic polymer," Science **298,** 1401-1403 (2002).
2. Y.Q. Shi, C. Zhang, H. Zhang, J.H. Bechtel, L. R. Dalton, B.H. Robinson, W.H. Steier, "Low (sub-1-volt) halfwave voltage polymeric electro-optic modulators achieved by controlling chromophore shape," Science **288,** 119-122 (2000).
3. Y. Enami, C.T. Derose, D. Mathine, C. Loychik, G. Greenlee, R.A. Norwood, T.D. Kim, J. Luo, Y. Tian, A.K.Y. Jen, N. Peyghambarian, "Hybrid polymer/sol-gel waveguide modulators with exceptionally large electro-optic coefficients," Nature Photonics **1,** 180-185 (2007).
4. H. Tazawa, W.H. Steier, "Analysis of ring resonator-based traveling-wave modulators," IEEE Photon. Technol. Lett. **18,** 211-213 (2006).
5. B. Bortnik, Y.C. Hung, H. Tazawa, B.J. Seo, J.D. Luo, A.K.-Y. Jen, W.H. Steier, H.R. Fetterman, "Electrooptic polymer ring resonator modulation up to 165 GHz," IEEE J. Sel. Top. Quantum Electron. **13,** 104-110 (2007).
6. P. Rabiei, W.H. Steier, Z. Cheng, and L.R. Dalton, "Polymer microring filters and modulators," J. Lightwave Technol. **20,** 1968-1975 (2002).
7. H. Tazawa, Y.-H. Kuo, I. Dunayevskiy, J.D. Luo, A.K.-Y. Jen, H.R. Fetterman, W.H. Steier, "Ring resonator-based electrooptic polymer traveling-wave modulator," J. Lightwave Technol. **24,** 3514-3519 (2006).

#88417 - $15.00 USD Received 14 Nov 2007; revised 4 Jan 2008; accepted 4 Jan 2008; published 8 Jan 2008

8. Q.F. Xu, B. Schmidt, S. Pradhan, M. Lipson, "Micrometre-scale silicon electro-optic modulator," Nature **435,** 325-327 (2005).
9. D. Rezzonico, A. Guarino, C. Herzog, M. Jazbinsek, P. Günter, "High-finesse laterally coupled organic-inorganic hybrid polymer microring resonators for VLSI photonics," IEEE Photon. Technol. Lett. **18,** 865-867 (2006).
10. I.L. Gheorma, R.M. Osgood, "Fundamental limitations of optical resonator based on high-speed EO modulators," IEEE Photon. Technol. Lett. **14,** 795-797 (2002).
11. B.E.A. Saleh, M.C.Teich, *Fundamental of Photonics* (Wiley, 1991).
12. K. Okamoto, *Fundamentals of Optical Waveguides* (Academic, 2000).
13. M.K. Smit, E.C.M. Pennings, H. Blok, "A normalized approach to the design of low-loss optical wave-guide bends," J. Lightw. Technol. **11,** 1737-1742 (1993).
14. T.D. Kim, J. Luo, J.W. Ka, S. Hau, Y. Tian, Z. Shi, N.M. Tucker, S.H. Jang, J.W. Kang, and A.K.Y. Jen,"Ultralarge and Thermally Stable Electro-optic Activities from DielsAlder Crosslinkable Polymers Containing Binary Chromophore Systems," Adv. Mater. **18,** 3038-3042 (2006)
15. U. Fano, "Effects of configuration interaction on intensities and phase shifts," Phys. Rev. **124,** 1866-1878 (1961).
16. Y. Lu, J. Yao, X. Li, P. Wang, "Tunable asymmetrical Fano resonance and bistability in a microcavity-resonator-coupled Mach-Zehnder interferometer," Opt. Lett. **30,** 3069-3071 (2005).
17. P.P. Absil, J.V. Hryniewicz, B.E. Little, R.A. Wilson, L.G. Joneckis, P.T. Ho, "Compact microring notch filters," IEEE Photon. Technol. Lett. **12,** 398-400 (2000).
18. A. Leinse, M.B.J. Diemeer, A. Rousseau, A. Driessen, "A novel high-speed polymeric EO modulator based on a combination of a microring resonator and an MZI ," IEEE Photon. Technol. Lett. **17,** 2074-2076 (2005).
19. S.H. Fan, "Sharp asymmetric line shapes in side-coupled waveguide-cavity systems," Appl. Phys. Lett. **80,** 908-910 (2002).
20. C.Y. Chao, L.J. Guo, "Biochemical sensors based on polymer microrings with sharp asymmetrical resonance," Appl. Phys. Lett. **83,** 1527-1529 (2003).
21. D. Rezzonico, M. Jazbinsek, P. Günter, Ch. Bosshard, D.H. Bale, Y. Liao, L.R. Dalton, P.J. Reid, "Photostability studies of π-conjugated chromophores with resonant and nonresonant light excitation for long-life polymeric telecommunication devices," J. Opt. Soc. Am. B **24,** 2199-2207 (2007).
22. A. Galvan-Gonzalez, M. Canva, G.I. Stegeman, L. Sukhomlinova, R.J. Twieg, K.P. Chan, T.C. Kowalczyk, H.S. Lackritz, "Photodegradation of azobenzene nonlinear optical chromophores: the influence of structure and environment," J. Opt. Soc. Am. B **17,** 1992-2000 (2000).
23. P. Prêtre, P. Kaatz, A. Bohren, P. Günter, B. Zysset, M. Ahlheim, M. Stähelin, F. Fehr, "Modified polyimide side-chain polymers for electrooptics," Macromolecules **27,** 5476-5486 (1994).
24. A. Guarino, G. Poberaj, D. Rezzonico, R. Degl'Innocenti, P. Günter, "Electro-optically tunable microring resonators in lithium niobate," Nature Photonics **1,** 407-410 (2007).

1. Introduction

The growing demand on telecommunication systems allowing for real-time multimedia streaming makes polymeric devices interesting for electro-optic modulation with bandwidths beyond 100 GHz. Due to their low dielectric loss and permittivity, reducing both electric attenuation and velocity mismatch between electric driving signals and optical carrier waves, polymeric devices are very promising candidates to suit the technological requirements for next generation high speed optical communications [1–3].

In the last few years, excellent modulation bandwidths and driving voltages have been demonstrated in centimeter-scale polymeric Mach-Zehnder interferometers (MZI) [1–3]. Despite this well established device technology, microring resonators have been shown to have the potential of higher miniaturization, better velocity mismatch tolerances and therefore larger bandwidths than MZI [4]. Polymeric microring resonators, as insulating dielectrics, are advantageous because of the electronic nature of the electro-optic (EO) response preserving the modulation performances beyond 100 GHz [5] and often require simpler technological prerequisites for the fabrication of the devices if compared to semiconductors (e.g., see [6]). Nevertheless, there are still some restrictions in terms of size reduction and dimensions of functional elements [7], while semiconductor-based ring resonators have already been demonstrated in micrometer-scale [8]. Among the major issues associated with EO polymeric ring-like devices, the usually small refractive index contrast between core and cladding makes bending losses non-negligible for curvature radii smaller than 100 μm. Also physicochemical compatibilities,

#88417 - $15.00 USD Received 14 Nov 2007; revised 4 Jan 2008; accepted 4 Jan 2008; published 8 Jan 2008

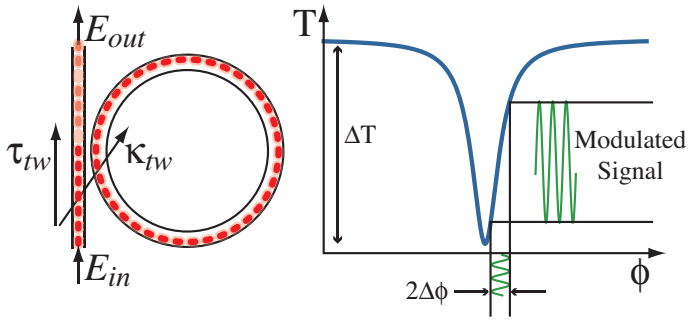

Fig. 1. *Left:* Scheme of a traveling wave resonator with lossless coupler. κ_{tw} is the amplitude coupling constant and τ_{tw} is the amplitude transmission constant, where $\kappa_{\mathrm{tw}}^2 + \tau_{\mathrm{tw}}^2 = 1$. *Right:* Operation principle of a resonator-based EO modulation. ΔT is the resonator signal extinction, while $\Delta\phi$ is the EO induced round-trip phase modulation amplitude.

technological features necessary for precise structuring [9], and successful, stable poling of the active compound in microstructures are generally challenging.

In this work, we introduce, design, model and produce EO polymeric microring modulators coupled to the bus waveguide by means of a so-called *Charon* coupler. In Section 2, we give a glance to the quantities characterizing a cavity-based EO modulator, particularly considering modulation sensitivity and bandwidth limitations, emphasizing the fabrication restrictions to overcome, for producing high performance modulators. In Section 3, we will show that *Charon* microresonators exhibit resonances with high extinction peaks *and* dips, whose shape is either symmetric Lorentzian or sharp and asymmetric. In Section 4, we present the experimental demonstration of such microresonators by micro-embossing and in Section 5 we analyze their spectral and EO characteristics. The presented approach provides better design freedom of the microring devices and can be regarded as a potential breakthrough towards further miniaturization of polymeric integrated optics systems.

2. Ring-like cavities as electro-optical modulators

A ring-shaped optical cavity coupled to a single bus waveguide (Fig. 1, left), also known as *traveling wave resonator* [10], has an intensity transmission function (e.g., see [4])

$$T(\phi) = \left|\frac{E_{\mathrm{out}}}{E_{\mathrm{in}}}\right|^2 = 1 - \frac{(1-\xi^2)(1-\tau_{\mathrm{tw}}^2)}{(1-\tau_{\mathrm{tw}}\xi)^2 + 4\tau_{\mathrm{tw}}\xi\sin^2(\phi/2)}. \tag{1}$$

In Eq. (1), ϕ is the round-trip phase change, ξ the amplitude round-trip loss factor, and τ_{tw} the cavity-bus waveguide amplitude transmission constant. The extinction at resonance $\Delta T \equiv T_{\max} - T_{\min}$ reaches its maximum in case of *critical coupling,* for that $\tau_{\mathrm{tw}} = \xi$.

The *finesse* of the resonator $\mathscr{F} \equiv \pi\sqrt{\tau_{\mathrm{tw}}\xi}/(1-\tau_{\mathrm{tw}}\xi)$ is used to write Eq. (1) in form of

$$T(\phi) = 1 - \frac{T_R}{1 + \left(\frac{2\mathscr{F}}{\pi}\right)^2 \sin^2(\phi/2)}, \tag{2}$$

where $T_R \equiv (1-\xi^2)(1-\tau_{\mathrm{tw}}^2)/(1-\tau_{\mathrm{tw}}\xi)^2 = 1 - T_{\min}$ is equal to one in case of critical coupling. $\mathscr{F}$ relates the free spectral range to the resonator linewidth $\delta\phi$ through

$$\mathscr{F} \approx \frac{2\pi}{\delta\phi}.$$

#88417 - $15.00 USD Received 14 Nov 2007; revised 4 Jan 2008; accepted 4 Jan 2008; published 8 Jan 2008

The finesse is a direct indication of the sharpness of the resonance lines with respect to their spectral separation, giving a measure of the cavity's quality. The often reported finesse of the unloaded resonator ($\mathscr{F}_{\mathrm{ul}} = \pi\sqrt{\xi}/(1-\xi)$) is a common way to express cavity losses.

The modification of the round-trip phase change

$$\Delta\phi = \frac{2\pi}{\lambda}\Big(-\frac{n^3}{2} r_{\mathrm{eff}} \frac{V_m}{d}\Big) L, \tag{3}$$

through the electro-optic effect, applying a modulation Voltage V_m, results in an amplitude modulation of the signal transmitted by the resonator (Fig. 1, right). The quantities $\lambda, n, r_{\mathrm{eff}}, d, L$ in Eq. (3) are the optical wavelength in vacuum, the effective refractive index, the effective electro-optic coefficient (including the optical/modulating field overlap coefficient), the electrode distance, and the ring circumference, respectively.

2.1. Modulation characteristics and limitations

Large signal switching by low voltage modulation is possible by setting the (phase) working point ϕ_o where the transmission curve's slope $\mathrm{d}T/\mathrm{d}\phi$ is largest. It can be easily shown from Eq. (2) that the maximum slope is proportional to $\mathscr{F}$ and holds

$$\left|\frac{\mathrm{d}T}{\mathrm{d}\phi}\right|_{\max} = \frac{3\sqrt{3}}{8}\frac{T_R}{\pi}\mathscr{F}, \tag{4}$$

at $\phi_o = \pm\sqrt{3}\pi/(3\mathscr{F}) \bmod 2\pi$. In case of critical coupling ($\tau_{\mathrm{tw}} = \xi$), T_R is equal to one and $|\mathrm{d}T/\mathrm{d}\phi|_{\max} \approx \mathscr{F}/5$. The consequence is that high modulation efficiency requires a large resonator finesse and the modulation sensitivity, expressed in terms of resonator *equivalent half wave voltage* [7]

$$V_\pi^{eq} = \frac{\pi}{2}\frac{1}{|\frac{\mathrm{d}T}{\mathrm{d}V}|_{\max}} = \frac{\pi}{2}\frac{1}{|\frac{\delta\phi}{\delta V}\frac{\mathrm{d}T}{\mathrm{d}\phi}|_{\max}}, \tag{5}$$

is inversely proportional to $\mathscr{F}$. The quantity $\delta\phi/\delta V$ in Eq. (5) defines the *tuning sensitivity* of the device.

On the other hand, $\mathscr{F}$ sets a fundamental limitation to the maximal modulation speed. In fact, even if polymeric microrings are good candidates for compact high speed EO modulation because of their material characteristics, for switching frequencies over today's standard 10 GHz, microring resonators show intrinsic dynamics limitations due to photon cavity lifetimes τ_{cav}, regardless of material EO sensitivities. If τ_{tw} and ξ are close to one, the resonator has a large finesse that is directly proportional to the photon cavity lifetime as [11]

$$\tau_{\mathrm{cav}} \approx \frac{nL}{2\pi c}\mathscr{F}. \tag{6}$$

Therefore, the available (optical) bandwidth $f_{3\mathrm{dB}}^{opt} \equiv 1/(2\pi\tau_{\mathrm{cav}})$ is inversely proportional to the finesse. Eqs. (4) and (6) demonstrate that there is a trade-off between fast and efficient EO modulation: high quality resonators with a large finesse allow for high signal extinctions by low voltage modulations but simultaneously severely limit the available modulation bandwidth.

Furthermore, as shown in the following paragraph (Section 2.2), for ring cavities with radii shrinking below $100\,\mu$m, the coupling efficiency is strongly reduced, among others, by the insufficient field interaction length at the coupler, so that micrometer-scale ring resonators are usually undercoupled ($\tau_{\mathrm{tw}} > \xi$). For cavities with the coupling constant $\kappa_{\mathrm{tw}} = \sqrt{1-\tau_{\mathrm{tw}}^2} \sim 0$, the photons hardly enter and exit the resonator, so that τ_{cav} is increased and the resulting bandwidth is further limited. Additionally, if the spectrum is asymmetric or $T_{\max} \ll 1$, a meaningful calculation of the photon cavity lifetime is only possible by evaluating the inverse Fourier transform of the resonances (see Section 5).

#88417 - $15.00 USD Received 14 Nov 2007; revised 4 Jan 2008; accepted 4 Jan 2008; published 8 Jan 2008

2.2. *Coupling performance and limitations*

The two parameters characterizing the resonator performances are the cavity losses, represented by the amplitude round-trip loss factor ξ, and the coupling constant κ_{tw}. While the former is mostly given by the cavity quality alone, the latter depends more on the design of the coupling region between bus and resonator waveguides.

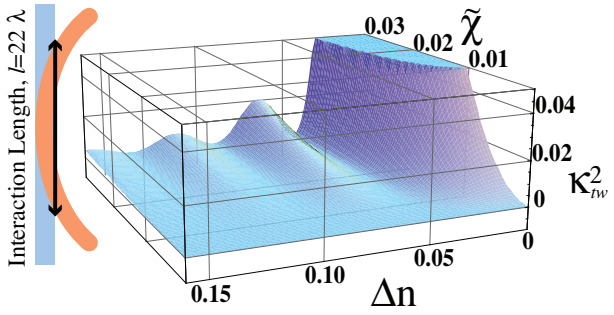

Fig. 2. Vertical power coupling κ_{tw}^2 between a straight and a 32λ-radius bent waveguide (corresponding to a radius of $50\,\mu$m for a wavelength $\lambda = 1.55\,\mu$m) as a function of the effective index difference Δn and the mode overlap coupling coefficient χ, expressed through the dimensionless parameter $\tilde{\chi} \equiv \chi\lambda$. The calculations are made by perturbation theory assuming a homogeneous field interaction along the whole interaction length $l = 22\lambda$.

The absolute power coupling κ_{tw}^2, as a function of the interaction length l between the optical fields in two adjacent waveguides, can be calculated through coupled-mode theory based on a perturbation approximation as [12]

$$\kappa_{tw}^2(l) = P\sin^2(ql), \tag{7}$$

where $q = \sqrt{[\chi^2 + 4\Delta\beta^2]}$ is the spatial coupling frequency and $P = (\chi/q)^2$ the maximal coupling efficiency. The coupling parameter χ is defined by mode overlap integral, while $\Delta\beta = (2\pi/\lambda)\Delta n$ is the propagation constant mismatch due to the effective index difference Δn between the waveguides. In Fig. 2, we present the calculated dependence of κ_{tw}^2 on the dimensionless coupling parameter $\tilde{\chi} \equiv \chi\lambda$ for a fixed interaction length l (in units of λ), and we use Δn as second free parameter; we chose these parameters for generality purposes.

For a given mode overlap $\tilde{\chi}$, the presence of $\Delta n \neq 0$ increases the spatial coupling frequency, making the patterned interaction length l, due to fabrication tolerances, inaccurate for effective coupling. Simultaneously, Δn reduces considerably the maximal coupling efficiency P. The difference between the effective refractive indices of bus and ring waveguides can severely limit the absolute power coupling and makes the cavity useless for amplitude modulation purposes. For polymeric devices, the absolute power coupling κ_{tw}^2 between a single-mode straight waveguide and a 32λ-radius bent waveguide with different effective indices, is well below 0.01 in a usual operating regime ($\tilde{\chi} < 0.01$ [12]; Fig. 2). The source of Δn may be solely due to the difficulties to match the effective indices of straight and curved structures [13], but Δn is more significant if two independent materials for bus and ring waveguides are used. We believe that the coupling dependence on the effective index difference Δn is a severe limitation which affects primarily the spectral response of the resonator and finally compromises the modulation effectivity of the device. Therefore, for sufficient coupling between an EO ring and a passive port channel, one needs to significantly modify the field interaction region to enhance the coupling of light to the ring.

#88417 - $15.00 USD Received 14 Nov 2007; revised 4 Jan 2008; accepted 4 Jan 2008; published 8 Jan 2008

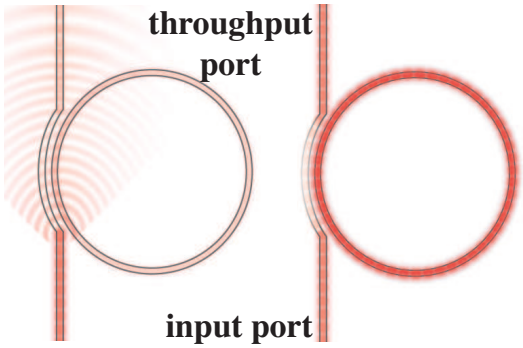

Fig. 3. Operation principle of a *Charon* microresonator. Out of resonance (left), most of the light entering the coupler is lost due to the distortion of the bus waveguide. In resonance (right), the ring "carries" the light across the lossy coupler leading to intensity maxima at the throughput port.

In the following section, we propose a new coupler design that increases the coupling considerably and also helps to overcome the finesse trade-off that limits the modulation bandwidth of high-efficiency resonator-based modulators.

3. Charon microresonators

The microring modulator we propose and demonstrate, that we call *Charon*, is based on the control of the losses in the coupling region, leading to an unexpected spectral behavior of the resonator. We show that the coupling characteristics dramatically influence the shape of the resonance curve at the throughput port. It may result in either spectra with Lorentzian peaks instead of dips, or strongly asymmetric spectra, leading to several advantages regarding coupling tolerances, resonance sharpness and tuning sensitivity.

The concept of the *Charon* microring resonator is depicted in Fig. 3. The bus waveguide is deformed so that, out of resonance (Fig. 3, left), the intensity at the throughput port is reduced, but the coupling to the ring is enhanced because the waveguides are merged. A significant portion of the light enters the ring but, since it is out of resonance, after a round trip interferes destructively with the entering light. In resonance, however (Fig. 3, right), the whispering gallery mode interferes constructively, resulting in an increase of the optical power stored in the ring, which is partially released into the bus waveguide at the throughput port. The ring acts therefore as a bandpass filter, collecting light at resonance from the input port and carrying it to the throughput port. The role of the *Charon* microring resonator is similar to that of the ferryman *Charon* in Greek mythology, taking souls across the river *Acheron,* and suggests, therefore, its name.

For the description of the *Charon* microring, we model the resonator spectral behavior introducing a special coupler consisting of three parts: two lossless partial couplers separated by a lossy field propagation region (see Fig. 4). The partial couplers are considered ideal, i.e. short enough so that the phase shift due to different propagation constants in the bus and the ring waveguide can be neglected. For the calculation of the transmitted field at the throughput port D as a function of the incoming field at the input port A, we use an amplitude-coupling matrix method. We first consider the incoming optical fields A from the input port and a from the resonator, passing the first partial coupler and being divided into the fields B and b. The optical waves B and b represent the fields in the two different arms of the *Charon* coupler immediately after the first partial coupler. The linear relation between (B,b) and (A,a) is given in matrix form

#88417 - $15.00 USD Received 14 Nov 2007; revised 4 Jan 2008; accepted 4 Jan 2008; published 8 Jan 2008

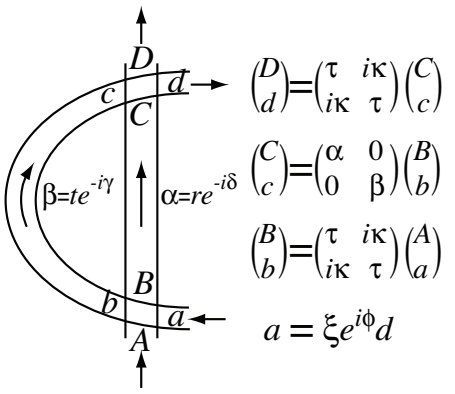

Fig. 4. Scheme of a *Charon* coupler between a straight waveguide and a microring resonator. The model of the coupler consists of three parts: two lossless partial couplers along with a lossy propagation region. The amplitude coupling constant κ and the transmission factor τ at the two partial couplers are real and must guarantee energy conservation, $\kappa^2+\tau^2=1$. The field loss factor of the cavity is ξ, while ϕ is the resonator round-trip phase change. The relations between the different optical field amplitudes are expressed in matrix form.

in Fig. 4. The amplitude coupling and transmission constants for the partial couplers are κ and τ, respectively; ideally, they are real quantities and fulfill energy conservation, $\kappa^2+\tau^2=1$ since we assume that all losses of the entire *Charon* coupler occur in the propagation region between the partial couplers. Eventual reflections and scattering at the partial couplers may affect the input/output efficiency of the device, but not the shape of the transmission spectrum. Note that κ and τ are not directly related to the coefficients κ_{tw} and τ_{tw} of a classical, weakly coupling, "single-element" directional coupler as introduced in Section 2. The optical fields B and b propagate toward the second partial coupler experiencing losses and phase shifts, described by $\alpha = r\exp(-i\delta)$ along the straight arm of the *Charon* coupler and $\beta = t\exp(-i\gamma)$ within its bent arm. The resulting fields $C = r\exp(-i\delta)B$ and $c = t\exp(-i\gamma)b$ couple in the second partial coupler. At the exit of the *Charon* coupler, the field D enters the throughput port waveguide, while d reaches the cavity. Within the ring resonator, the whispering gallery mode d propagates through the cavity, undergoing amplitude losses ξ and a round-trip phase shift ϕ before entering the *Charon* coupler again. Therefore, the field a can be expressed with the field d after propagation along the ring circumference, as $a = \xi\exp(i\phi)d$.

The transmission function of the resonator $T = |D/A|^2$ is calculated from the product of matrices

$$\begin{pmatrix} D \\ d \end{pmatrix} = \begin{pmatrix} \tau & i\kappa \\ i\kappa & \tau \end{pmatrix} \begin{pmatrix} \alpha & 0 \\ 0 & \beta \end{pmatrix} \begin{pmatrix} \tau & i\kappa \\ i\kappa & \tau \end{pmatrix} \begin{pmatrix} A \\ a \end{pmatrix}. \tag{8}$$

For T, one finds:

$$T(\phi) = \left| \alpha(1-\kappa^2) - \beta\kappa^2 - \frac{(\alpha+\beta)^2\kappa^2(1-\kappa^2)\xi e^{i\phi}}{1+(\alpha\kappa^2-\beta(1-\kappa^2))\xi e^{i\phi}} \right|^2. \tag{9}$$

Eq. (9) depends on one hand on intrinsic cavity losses ξ and on the other hand on the parameters of the *Charon* coupler: the (partial) coupling constant κ; the losses r and t, as well as the phase shifts experienced within the coupler's arms δ and γ, respectively.

Since the simultaneous control of all parameters is very difficult, we consider the following approximation. The bent arm of the *Charon* coupler belongs to the ring resonator, therefore, the

#88417 - $15.00 USD Received 14 Nov 2007; revised 4 Jan 2008; accepted 4 Jan 2008; published 8 Jan 2008

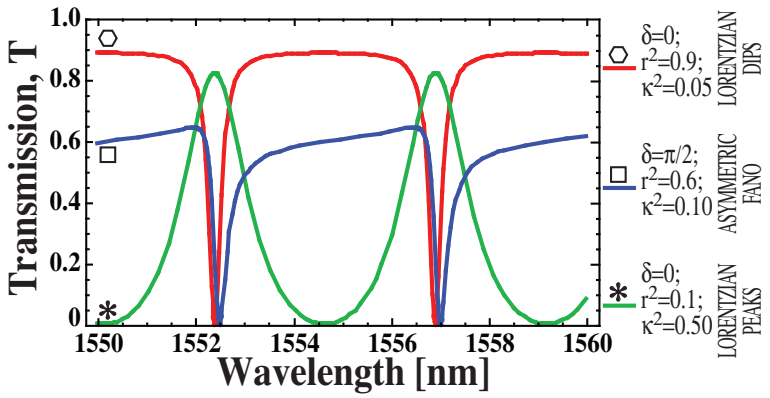

Fig. 5. Throughput port transmission characteristics of *Charon* microresonators for partial coupler energy exchange coefficients $\kappa^2 = [0.05, 0.1, 0.5]$, energy coupler loss parameters $r^2 = [0.9, 0.6, 0.1]$ an phase asymmetry $\delta = [0, \pi/2, 0]$, respectively. Slope, extinction and insertion loss for these curves are marked with the corresponding symbol in Fig. 7. All curves are calculated for an amplitude resonator loss factor $\xi = 0.9$, ring radius $R = 50\,\mu$m and effective refractive index $n_{\text{eff}} = 1.7$.

bent arm losses t and phase shifts γ are included in the cavity counterparts ξ and ϕ, respectively. This way, $\beta = 1$ and the effects of the *Charon* coupler are assumed only by the straight arm with its losses r and phase shift δ, together with the partial coupling constant κ.

Depending on the values of κ, r and δ, such couplers can basically lead to three different throughput port transmission spectra: Lorentzian dips as for normal traveling wave resonators; Lorentzian peaks, otherwise typical for drop ports of add-drop microresonators; Fano resonances with strongly asymmetric resonances.

Lorentzian dips in the throughput port transmission spectrum obviously appear if $\delta = 0$, $\kappa \ll 1$, and $r \to 1$ since this is the normal case of a traveling wave resonator with weak coupling and low insertion loss (Fig. 5, ⬡). Note that, if $r = 1$ and $\delta = 0$, a direct comparison between the "normal" transmission function as in Eq. (1) and the *Charon* transmission function in Eq. (9) is still possible after the substitutions $\tau_{\text{tw}} = \tau^2 - \kappa^2$ and $\kappa_{\text{tw}} = 2\kappa\tau$, since the cavity keeps its full symmetry. The same kind of curve is also observed if $\delta \neq 0$ for a cavity in a strong coupling regime (e.g. $\kappa^2 = 0.35$, see Fig. 6, ⋄). Due to the fact that $\alpha \neq 1$, a direct comparison of Eqs. (1) and (9) is not possible in this case.

Lorentzian peaks are observed in *Charon* microring transmission spectra in the occurrence, out of resonance, most of the light is lost at the coupler but the power exchange at the partial couplers is enhanced. For the example shown in Fig. 5, (∗), with $r^2 = 0.1$ and $\kappa^2 = 0.5$, the extinction ratio is still very high and the insertion loss (i.e. the power missing at the throughput port due to the losses at the coupler) is kept in the order of 0.2. The operation principle of this type of *Charon* devices has been heuristically explained in Fig. 3.

Fano resonances [15], having very steep edges, are realized with a moderately lossy coupler ($r^2 = 0.3$-0.6), where a coupler phase propagation mismatch ($\delta > 0$) leads to a strongly asymmetric spectrum (Fig. 5, □ and Fig. 6, ○).

As shown, the phase mismatch δ may not only be responsible for the asymmetry of the spectrum, but plays a decisive role also in case of strong coupling ($\kappa^2 = 0.35$) and low coupling losses ($r^2 = 1$): the velocity mismatch between the modes propagating in the two arms of the *Charon* coupler leads to high extinction, sharp resonances that were impossible with fields propagating at the same speed through the coupler (Fig. 6, compare ⋄ and ⋆). On the other hand,

#88417 - $15.00 USD Received 14 Nov 2007; revised 4 Jan 2008; accepted 4 Jan 2008; published 8 Jan 2008

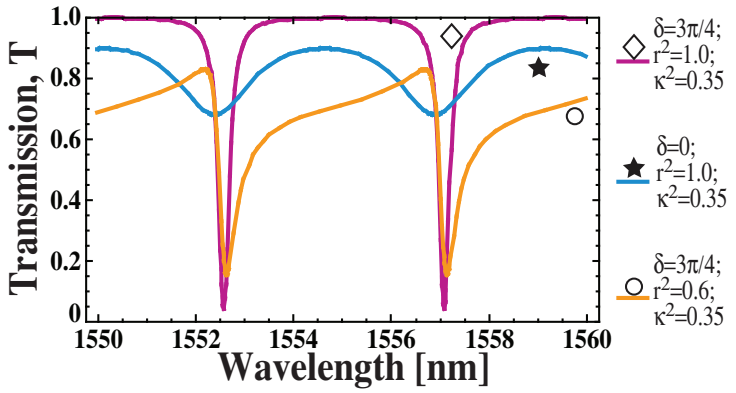

Fig. 6. *Charon* transmission spectrum dependence on the coupler phase-shift δ for over-coupled microresonators ($\kappa^2 = 0.35, \xi = 0.9$). The phase asymmetry $\delta = 3\pi/4\,(\diamond)$ increases the maximum slope $|\mathrm{d}T/\mathrm{d}\lambda|_{\max}$ by more than one order of magnitude as compared to $\delta = 0\,(\star)$. The photon lifetime of the lossy-coupler asymmetric resonator ($r^2 = 0.6$, $\circ$) is reduced by 30% with respect to the lifetime of a lossless-coupler asymmetric cavity ($r^2 = 1, \diamond$), but the maximum slopes are similar. Slope, extinction and insertion loss for these curves are marked with the corresponding symbol in Fig. 7.

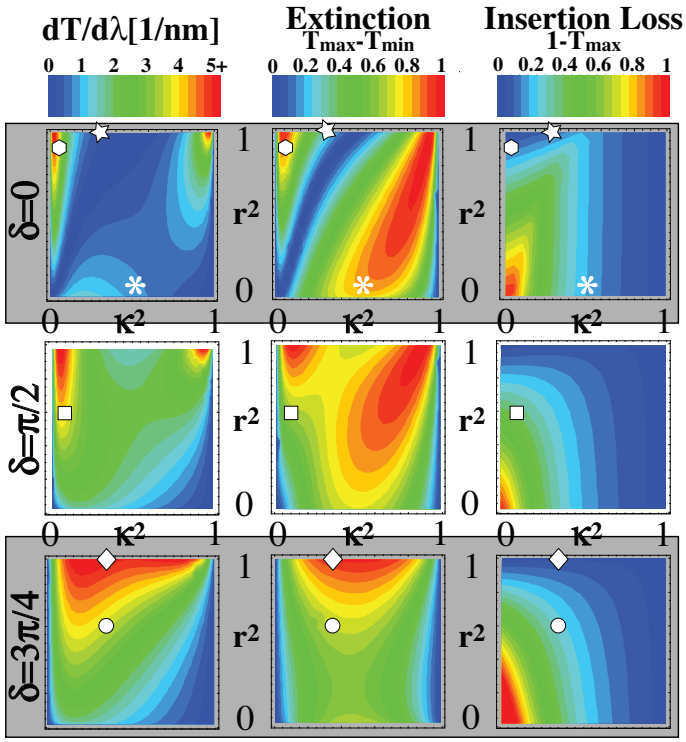

Fig. 7. Impact of the lossy *Charon* coupler on the slope $|\mathrm{d}T/\mathrm{d}\lambda|_{\max}$, the signal extinction $\Delta T = T_{\max} - T_{\min}$ and the insertion loss $1 - T_{\max}$ for three different coupler phase asymmetries $\delta = [0, \pi/2, 3\pi/4]$, varying energy coupling constants κ^2 and losses r^2, for a constant $\xi = 0.9$. The symbols $\hexagon, \star, *, \circ, \square$, and $\diamond$ represent the parameters for the spectra depicted in Figs. 5 and 6.

#88417 - $15.00 USD Received 14 Nov 2007; revised 4 Jan 2008; accepted 4 Jan 2008; published 8 Jan 2008

the losses at the coupler r^2 and the resulting enhanced coupling broaden the resonances and decrease the photon cavity lifetime, while the phase asymmetry δ ensures that at least one edge of the transmission resonance remains steep. This represents a fundamental advantage of our configuration: the modulation response can be increased without compromising the bandwidth by appropriately tuning of the parameters (r, δ, κ). The photon lifetimes τ_{cav} of the curves ($\diamond$) and ($\circ$) of Fig. 6 have been calculated by Fourier analysis: they are 4.9 ps for the former and 3.4 ps for the latter.

Depending on the application and the technological requirements, as well as limitations dictated by the fabrication techniques, the coupler can be designed to match the needed wavelength selectivity, maximum spectral slope, extinction ratio, available modulation bandwidths or insertion loss with larger tolerances by increasing the coupling acceptance through the phase asymmetry δ (see Fig. 7).

As an example we consider the following two cases for a 50-μm radius microring modulator, made of a material with an EO coefficient $r_{33} \sim 250$ pm/V [14], with reasonably low losses (amplitude loss parameter $\xi = 0.975$, corresponding to 7 dB/cm). If the coupler is as conventional, i.e. lossless and symmetric ($r = 1, \delta = 0$), the spectral slopes $dT/d\lambda$ needed for half wave voltages below $V_\pi = 1.3$V are reached for energy coupling parameters between $\kappa^2 = 0.002$ and $\kappa^2 = 0.015$ (Fig. 8). Alternatively, increasing δ up to $3\pi/4$ with coupling losses as low as $r^2 = 0.98$, the same V_π's are available for energy coupling constants from $\kappa^2 = 0.015$ to $\kappa^2 = 0.106$. For such devices, the choice of the phase asymmetry parameter δ enlarges the coupling acceptance by up to a factor of eight with respect to normal, lossless coupler resonators ($r^2 = 1, \delta = 0$).

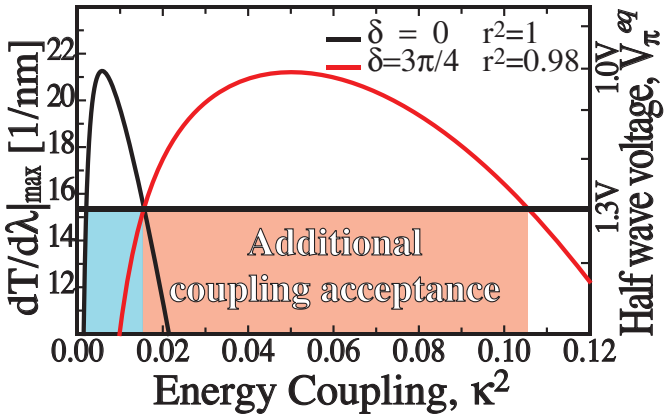

Fig. 8. Maximum spectral slope $|dT/d\lambda|_{max}$ and corresponding equivalent half wave voltage V_π^{eq} (see Eq. (5)) as a function of the energy coupling κ^2 for symmetric ($\delta = 0$) and strongly asymmetric ($\delta = 3/4\pi$) *Charon* couplers, respectively. The coupling acceptance for 1.3-V half wave voltage or better devices is increased from $\Delta\kappa^2 \sim 0.013$ (yellow shaded area) if $\delta = 0$ to $\Delta\kappa^2 \sim 0.091$ when $\delta = 3\pi/4$ (green shaded area). A nonlinear optical polymer with EO coefficient $r_{33} \sim 250$ pm/V [14] has been considered.

The spectral behavior of the asymmetric *Charon* microring is similar to the one of a resonant cavity coupled to a MZI, as proposed by Lu *et al.* [16] and realized by Absil *et al.* in GaAs [17] and lately by Leinse *et al.* in polymers [18]. The advantage of the *Charon* configuration is that there is no need for the "macroscopic" MZI, and the problems related to critical coupling can be avoided, especially if the waveguides are made of materials with much different refractive indices and if the interaction length at the coupler is particularly short. Sharply asymmetric line

#88417 - $15.00 USD Received 14 Nov 2007; revised 4 Jan 2008; accepted 4 Jan 2008; published 8 Jan 2008

shapes have also been suggested by Fan [19] through a combination of two lopsided cavities, and have been partially demonstrated by Chao and Guo [20] in passive polymeric racetrack structures.

4. Realization of *Charon* microring modulators

4.1. Material choice

The performance needed for EO modulator applications sets severe requirements on the compounds of a polymeric microring and limits the number of possible material combinations.

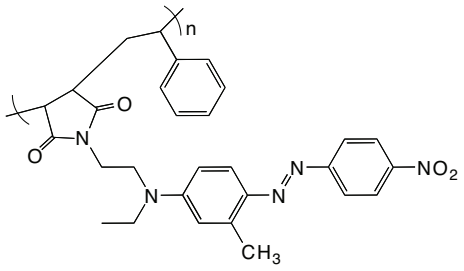

Fig. 9. Structure of the azo-stilbene based polyimide SANDM2.

The *core* EO polymer must have a high index of refraction of at least 1.65 to allow for bending radii as small as $50\,\mu$m, and a glass transition temperature T_g exceeding 150°C in order to keep the chromophore orientation for a long time [3]. It must be highly photostable for persistent strong conjugation of the active chromophores [21], and have an acceptable EO coefficient r_{33}.

All these characteristics were measured in films of the azo-stilbene based polyimide SANDM2 (see Fig. 9). SANDM2 exhibits $T_g \sim 175$°C, with refractive index $n = 1.67 \pm 0.02$, and EO coefficient $r_{33} = (8 \pm 2)$ pm/V, both at $\lambda = 1550$ nm wavelength. Its dielectric constant is $\varepsilon \sim 3.7$ at radio frequencies (rf) and it is known that azo-stilbenes experience almost no photo-oxidation and are particularly inert under optical irradiation [22]. Supplementary information on polymers of the same family of SANDM2 is available in the work of Prêtre *et al.* [23].

The *cladding* material should have a refractive index smaller than 1.5 along with a dielectric permittivity possibly higher than that of the core, so that the driving electric field is more concentrated in the active core material [1]. Additionally, the cladding must be mechanically and chemically stable, and its electric strength must exceed $100\,\text{V}/\mu$m for standing the poling procedure. Also, its combination with the core should allow for easy and precise structuring.

As a trade-off among the different characteristics, the UV curable hybrid polymer Ormocomp (Microresist Tech, Germany) is an ideal choice as cladding material. We determined the refractive index at telecommunication wavelengths $n = 1.50 \pm 0.01$, the dielectric constant is $\varepsilon \sim 3.9$ at rf, and we did not notice any breakdown for electric fields strengths in the order of $250\,\text{V}/\mu$m.

For technological reasons, low loss single mode bus waveguides were made of the photoresist SU-8, also from Microresist, having a refractive index of $n = 1.57 \pm 0.01$ at $\lambda = 1550$ nm.

4.2. Device fabrication

The devices were produced by micro-embossing technique. As substrate, highly p-doped silicon wafers with resistivity smaller than $0.05\,\Omega$cm were used, acting therefore also as lower electrodes. A 2-μm thick layer of silicon dioxide at the surface served as index barrier to the

#88417 - $15.00 USD Received 14 Nov 2007; revised 4 Jan 2008; accepted 4 Jan 2008; published 8 Jan 2008

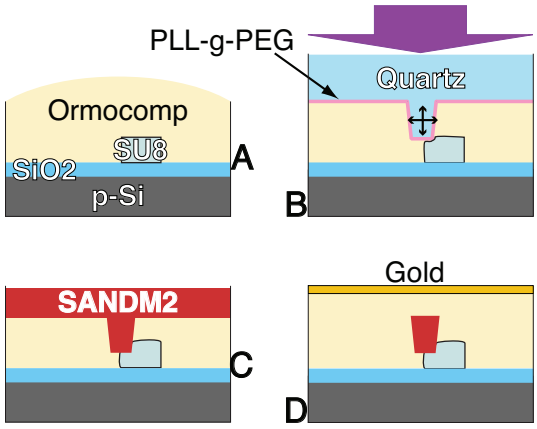

Fig. 10. Schematic patterning procedure. (A) The straight bus waveguides of SU-8 were directly written by standard photolithography and covered by the cladding resin Ormocomp. (B) The quartz mold with the microrings was pressed against the sample, structuring the rings in form of grooves. Alternatively, either a deformation or a displacement of the bus waveguides occurred by slight shifting of the stamp in contact with the SU-8 structures and the patterns were fixed by UV exposure. The PPL-g-PEG coating allowed for clean removal of the stamp from the molded Ormocomp layer. (C) The sample was coated with the electro-optic polymer SANDM2 to fill the grooves. After vacuum drying, the excess layer was removed by RIE. (D) The devices were covered with a cladding layer and a gold top electrode.

substrate. The single mode port waveguides, produced by direct photolithography of the photoresist SU-8, having a cross section of $3.5 \times 2\,\mu\text{m}^2$, were covered with the cladding resin Ormocomp (Fig. 10, A). The 50-μm radius microrings were molded into the Ormocomp in form of grooves using a series of previously structured quartz plates as stamps. These were treated with a thin layer of graft co-polymer PLL-g-PEG (Susos, Switzerland) inhibiting the adhesion of the resin to the plate. Being a crucial step of the device production, our specially developed micro-embossing technique allows to pattern the microrings without damage and simultaneously create the deformation at the bus waveguide needed to enhance coupling at the *Charon* coupler (Fig. 10, B). The patterned Ormocomp with the ring-like grooves was then solidified by UV exposure and hard cured in the oven. The trenches were filled by repeated spin coatings of a dense solution of SANDM2 in TCE and completely dried in vacuum (Fig. 10, C). The SANDM2 film thickness in excess was etched down by oxygen plasma. The samples were then coated by a cover film of $2\,\mu$m of Ormocomp followed by a deposition of a gold layer acting as top electrode (Fig. 10, D). The resulting devices had a distance between the electrodes of 5 to $7\,\mu$m. Finally, the SANDM2 rings were poled slightly below T_g with a field of about $100 V/\mu$m for 1 hour. The samples were cleaved in order to allow for end-fire coupling during characterization experiments. Pictures of the produced couplers, showing two different deformations achieved, are presented in Figs. 11 and 12.

5. Experimental characterization of electro-optic *Charon* microring modulators

The electro-optic microring resonators were characterized by transmission and electro-optic modulation experiments using TE and TM polarized light from the tunable laser diode Santec TSL-220 focussed onto the input facets of the input bus waveguides. The transmitted spectrum was collected by a photodiode. The top electrode on the sample was contacted using a needle

#88417 - $15.00 USD Received 14 Nov 2007; revised 4 Jan 2008; accepted 4 Jan 2008; published 8 Jan 2008

while the bottom electrode was grounded by partially removing the oxide layer from the lower face of the silicon wafer and covering it with silver paint. The spectral characterization was performed by scanning the wavelength within the telecommunication C-band and recording the transmission. A reference straight waveguide was used to estimate the losses introduced by the *Charon* coupler. Modulation experiments were performed by applying a sinusoidal electric signal to the electrodes (2 V peak-to-peak amplitude in the kilohertz range), and measuring the amplitude modulation with a lock-in amplifier. The function generator and lock-in amplifier used were an Instek GFG-8219 and a Stanford SR830, respectively.

The measured TE spectrum of 50-μm radius microresonators made of SANDM2 surrounded by Ormocomp, with *laterally* distorted *Charon* coupler is shown in Fig. 11. It exhibits almost symmetric high extinction ratio resonance peaks (about 11 dB). The analysis of the presented measurement shows a round-trip loss factor $\xi = 0.93$, corresponding approximatively to ring losses of 20 dB/cm, and a phase asymmetry $\delta = 1.7$ rad. The power coupling at the partial coupler κ^2 is enhanced by the bow of the *Charon* coupler to a value approaching 0.4. The coupler loss factor due to the lateral deformation in the coupling region is $r^2 = 0.03$ and the transmission's maximum slope $|\mathrm{d}T/\mathrm{d}\lambda|_{\max}$ about $1.7\,\mathrm{nm}^{-1}$! Despite the low value of r^2, the total insertion loss $1 - T_{\max}$ can be quantified into 1 dB because the coupling is very strong and, at resonance, about 80 % of the light is carried by the *Charon* resonator to the throughput port.

In Fig. 12, we present the transmission experiments done with *vertically* coupled *Charon* microrings exhibiting both TE and TM (not shown) spectra with strongly asymmetric Fano resonances. The analysis of the TE spectrum reveals a phase asymmetry $\delta = 2.0$ rad, power coupling $\kappa^2 = 0.07$, round-trip loss factor $\xi = 0.9$ with a coupler energy loss factor r^2 of 0.4, and extinction ratio of 7 dB. The absolute maximum slope is around $4.65 \times 10^4\,\mathrm{W/(cm^2 nm)}$ that corresponds to $|\mathrm{d}T/\mathrm{d}\lambda|_{\max} = 3.4\,\mathrm{nm}^{-1}$. The total insertion loss for TE polarized light is about 3 dB. The cavity photon lifetime of the device, $\tau_{\mathrm{cav}} = 5.5$ ps, has been determined

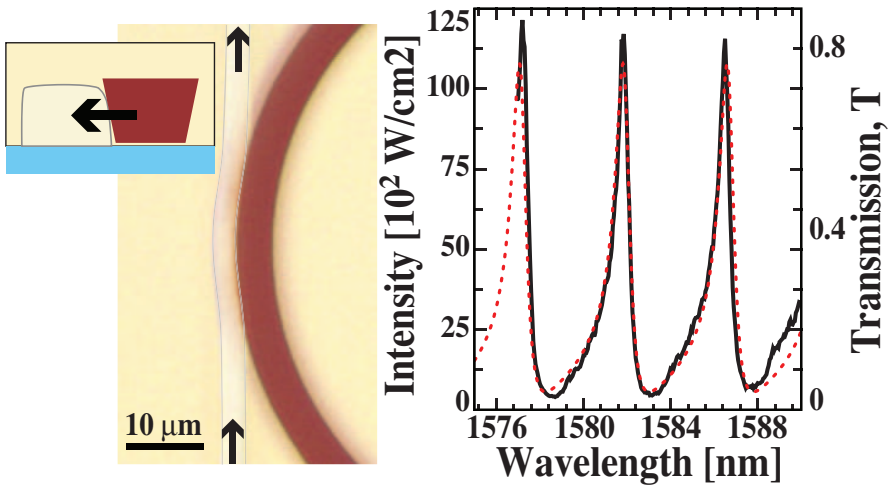

Fig. 11. Laterally coupled *Charon* microring. *Left:* Microscope picture of a lateral *Charon* microring's coupler with front-view scheme. The lateral displacement of the bus waveguide is induced by a horizontal shift of the molding stamp. The rings had a radius of 50 μm and a trapezoidal cross section with bases of 3 and 5 μm, respectively, while their height was 2 μm. *Right:* Measured TE transmitted intensity (solid line, left scale) and the corresponding analytical curve according to Eq. (9) (dotted line, right scale) showing high extinction peak-like resonances. The curve parameters are: $\delta = 1.7$ rad, $\kappa^2 = 0.4, r^2 = 0.03$.

#88417 - $15.00 USD Received 14 Nov 2007; revised 4 Jan 2008; accepted 4 Jan 2008; published 8 Jan 2008

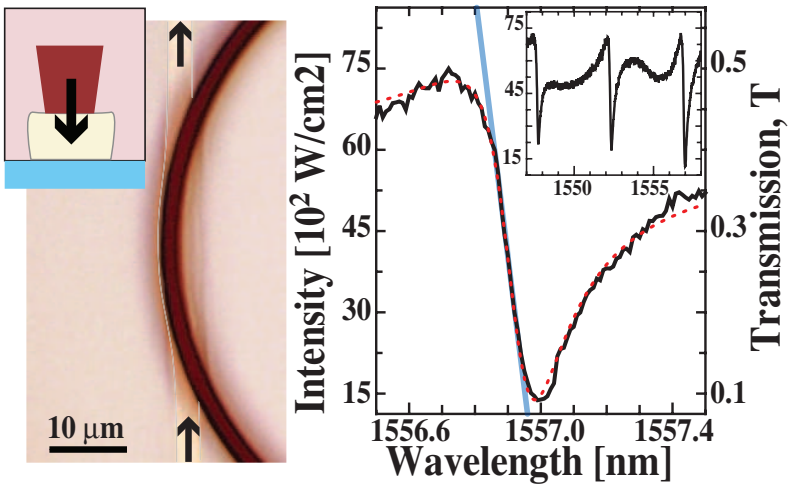

Fig. 12. Vertically coupled *Charon* microring. *Left:* Microscope view of a vertical *Charon* microring's coupler with front-view scheme. A deformation of the bus waveguide is produced by slightly excessive pressure of the mold. The 50-μm radius rings had a trapezoidal cross section with bases of 2 and 3 μm, respectively, and height of 2.7 μm. *Right:* Particular of the measured TE transmitted intensity (solid line, left scale) and the corresponding analytical curve according to Eq. (9) (dotted line, right scale), showing strongly asymmetric Fano resonances with approximately linear steepest resonance edge (blue straight line). The curve parameters are: $\delta = 2.0\,\mathrm{rad}$, $\kappa^2 = 0.07$, $r^2 = 0.4$. A wider portion of the spectrum is depicted in the inset.

by Fourier analysis of the resonances. The corresponding available modulation bandwidth is $f_{3\mathrm{dB}}^{opt} = 29\,\mathrm{GHz}$, which is by 30% larger than for a classical undercoupled traveling wave resonator showing the same maximum spectral slope.

The TM spectrum exhibits the following parameters: phase asymmetry $\delta = 2.5\,\mathrm{rad}$, power coupling $\kappa^2 = 0.17$, round-trip loss and insertion loss factors $\xi = 0.85$ and $r^2 = 0.5$, respectively. Due to the higher resonator losses, the extinction ratio is below 3 dB and the maximum transmission slope $|\mathrm{d}T/\mathrm{d}\lambda|_{\max}$ is about $1.9\,\mathrm{nm}^{-1}$, with an insertion loss of 2 dB. For the TM polarization, $\tau_{\mathrm{cav}} = 3.6\,\mathrm{ps}$, corresponding to $f_{3\mathrm{dB}}^{opt} = 43\,\mathrm{GHz}$ maximum modulation bandwidth.

These samples were used to perform preliminary electro-optic modulation experiments, in which the on-chip r_{33} value remained smaller than 1 pm/V, meaning that the material was nearly unpoled. Nevertheless, with non-optimized poling, the detected modulated signal showed a tuning sensitivity of 6.5 MHz/V for TM polarization and 4.3 MHz/V for TE polarized light. Through the constant derivative of the steepest resonance edge (blue straight line in Fig. 12), we calculated that the switch-over voltage needed to turn on the transmission from $T_{\min} = 0.1$ to $T_{\max} = 0.5$ was $V_{so} = 3.3\,\mathrm{kV}$. A complete poling can lead to an effective EO coefficient $r_{33} \sim 10\,\mathrm{pm/V}$, thus, we expect the performances of these polymeric microring modulators to be comparable with those we recently reported for ion-sliced thin-film lithium niobate microring resonators [24]. By substituting SANDM2 with the currently demonstrated best on-chip EO polymer AJC146 ($r_{33} \sim 150\,\mathrm{pm/V}$ on-chip) as presented by Enami *et al.* [3], one is able to reduce the switch-over voltage of the presented microring modulators below $V_{so} = 2\,\mathrm{V}$.

#88417 - $15.00 USD Received 14 Nov 2007; revised 4 Jan 2008; accepted 4 Jan 2008; published 8 Jan 2008

6. Conclusions

We have proposed and realized a new type of microring modulators, that we called *Charon,* based on a coupler with enhanced energy exchange. The suggested system allows to shape the resonator transmission curve at the throughput port to obtain Lorentzian dips, Lorentzian peaks, or asymmetric Fano resonances. Through the analysis of the *Charon* model, we demonstrated that the additional phase shift introduced by the coupler in the optical wave makes possible to produce 1-V half wave voltage micrometer-scale devices in spite of coupling tolerances and intrinsic propagation losses. The low V_π is possible by increasing the steepness of the transmission response still maintaining a larger bandwidth than for a comparable classical traveling wave microring resonator.

First 50-μm radius *Charon* polymeric electro-optic microring modulators made of the azostilbene based polyimide SANDM2 surrounded by the hybrid UV curable Ormocomp have been produced by micro-embossing. In a preliminary experiment, electro-optic modulation has been demonstrated, showing the advantages of the *Charon* structure also in terms of available modulation bandwidth. We are therefore persuaded that *Charon* microring resonators allow for a further miniaturization of (polymeric) electro-optic devices toward very large scale integration of optical circuits.

Acknowledgment

The authors would like to thank Dr. Christian Herzog and Dr. Riccardo Degl'Innocenti for the help in the measurement and for the preliminary materials characterization, Mathias Stahel for his contribution in the initial production procedure, Reto Gianotti for the EO polymer synthesis, as well as Dr. Samuele Tosatti with Dr. Stefan Zürcher for providing the PLL-g-PEG coating. This work has been supported by the Swiss National Science Foundation (200020-112148). At present, O-Pil Kwon is with the Department of Molecular Science and Technology, Ajou University, Suwon, 443-749, Korea.

#88417 - $15.00 USD Received 14 Nov 2007; revised 4 Jan 2008; accepted 4 Jan 2008; published 8 Jan 2008